

# Radiative corrections and quantum gates in molecular systems

John H. Reina,<sup>1</sup> Ray G. Beausoleil,<sup>2</sup> Tim P. Spiller,<sup>3</sup> and William J. Munro<sup>3</sup>

<sup>1</sup>*Centre for Quantum Computation, Physics Department, Oxford University, OX1 3PU, United Kingdom  
Materials Department, Oxford University, Oxford OX1 3PH, United Kingdom\**

<sup>2</sup>*Hewlett-Packard Laboratories, 13837 175<sup>th</sup> Pl. NE, Redmond, WA 98052-2180, USA*

<sup>3</sup>*Hewlett-Packard Laboratories, Filton Road, Stoke Gifford, Bristol BS34 8QZ, United Kingdom  
(Dated: September 29, 2018)*

We propose a method for quantum information processing using molecules coupled to an external laser field. This utilizes molecular interactions, control of the external field and an effective energy shift of the doubly-excited state of two coupled molecules. Such a level shift has been seen in the two-photon resonance experiments recently reported in Ref. [1]. Here we show that this can be explained in terms of the QED Lamb shift. We quantify the performance of the proposed quantum logic gates in the presence of dissipative mechanisms. The unitary transformations required for performing one- and two-qubit operations can be implemented with present day molecular technology. The proposed techniques can also be applied to coupled quantum dot and biomolecular systems.

PACS numbers: 03.67.Lx, 42.50.Fx, 32.80.Qk, 33.50.Dq

There is currently enormous interest in the field of quantum information processing (QIP). Potentially useful applications range from speeding up computations such as factoring, which would require tens of thousands of qubits, through searching and quantum simulations, which could be useful with a hundred or less, down to teleportation and quantum repetition of communication, which are effectively just few-qubit QIP. There have been some successful demonstrations of few qubit manipulations, and there exists a vast and still-growing range of proposals for realising QIP. The way forward is still very open—the key routes to few-qubit and large-scale QIP, which could well differ, have yet to be identified. Of particular interest are new proposals that are based on already observed phenomena, or that are clearly amenable to experimental investigation with current technology.

In this Letter we show how to use small quantum networks of coupled molecules to implement gate operations that enable universal QIP. A crucial ingredient to this is an effective energy shift of the doubly-excited state of two coupled molecules. We show that this can be explained in terms of the Lamb shifts of the levels, and we discuss how such a system can be tailored, with current technology, to realise a universal gate-set. We quantify the gate performance, and calculate molecular resonance fluorescence spectra for comparison with experiment. Although the physical origin of the relevant energy level shift will be (potentially) different, it is clear that the approach can also be applied to other systems, such as coupled self-assembled quantum dots or biomolecules.

We commence by describing our set-up. Consider two two-level closely spaced molecules fixed at positions  $\mathbf{r}_i$ , which have excitation frequencies  $\omega_i$ ,  $i = 1, 2$ , and are separated by the vector  $\mathbf{r}_{12}$ . The dipole-coupled molecules are embedded in a dispersive medium of refraction index  $n$  and interact with the quantized radiation field and with an external coherent driving field of fre-

quency  $\omega_L$ . Evidence of such dipole-dipole ( $d$ - $d$ ) coupling and the generation of sub and super-radiant states has recently been experimentally reported in a set-up that involves single terrylene molecules in a para-terphenyl crystal [1]. We denote the ground and excited molecular states by  $|g_i\rangle \equiv |0_i\rangle$ , and  $|e_i\rangle \equiv |1_i\rangle$ , with associated transition dipole moments  $\mathbf{d}_i$ , and corresponding spontaneous emission rates  $\Gamma_i$ . The strength of the molecule-laser coupling is given by  $\ell_i \equiv -\mathbf{d}_i \cdot \mathbf{E}_i$ , with  $\mathbf{E}_i$  being the amplitude of the coherent driving field at  $\mathbf{r}_i$ . The coupled molecules can be represented as a single four-level system in  $SU(4)$ ; we write the system interaction Hamiltonian in the computational basis of direct product states  $|i\rangle \otimes |j\rangle$  ( $i, j = 0, 1$ ) as

$$\hat{H} = [\hat{H}_0^{(1)} + \hat{H}_L^{(1)}] \otimes \hat{\mathbb{I}}^{(2)} + \hat{\mathbb{I}}^{(1)} \otimes [\hat{H}_0^{(2)} + \hat{H}_L^{(2)}] + \hat{H}_{12}, \quad (1)$$

where  $\hbar V_{12}$  denotes the  $d$ - $d$  interaction energy, and the free, laser, and interaction Hamiltonians are given by  $\hat{H}_0^{(i)} = \frac{\hbar\omega_i}{2}[\hat{P}_{22}^{(i)} - \hat{P}_{11}^{(i)}]$ ,  $\hat{H}_L^{(i)} = \hbar\ell^{(i)}[\hat{P}_{12}^{(i)}e^{i\omega_L t} + \hat{P}_{21}^{(i)}e^{-i\omega_L t}]$ ,  $\hat{H}_{12} = \hbar V_{12}[\hat{P}_{21}^{(1)} \otimes \hat{P}_{12}^{(2)}] + \hbar V_{12}^*[\hat{P}_{12}^{(1)} \otimes \hat{P}_{21}^{(2)}]$ , with  $\hat{P}_{ij} = |i\rangle\langle j|$  denoting the transition operators, and  $|i\rangle$  and  $|j\rangle$  being the eigenvectors spanning the Hilbert space. One can then map the transition operators into the pseudo-spin-1/2 dipole raising and lowering operators  $\hat{S}_i^\pm$ :  $\hat{S}_i^+ = \hat{P}_{21}^{(i)}$ ,  $\hat{S}_i^- = \hat{P}_{12}^{(i)}$ ,  $\hat{S}_i^+\hat{S}_i^- = \hat{P}_{22}^{(i)}$ , and  $\hat{S}_i^-\hat{S}_i^+ = \hat{P}_{11}^{(i)}$ , thus generating the corresponding operator algebra in  $SU(2) \otimes SU(2)$ . We allow for a detuning  $\Delta_i = \omega_i - \omega_L$  between the incident field and the molecular transitions. We also incorporate a shift  $\Delta_\epsilon$  of the doubly-excited state in our model—we shall show that this shift is an important feature of a robust molecular quantum gate. In our work we encode two qubits into this two-molecule system. Related work on such systems, where a single qubit is encoded into a molecular dimer, is discussed in reference [2]. In the following, we make use of the electric-dipole approximation  $k_0 r_{12} \ll 1$

( $ck_0 \equiv 2\pi\nu_0 = 2\pi(\nu_1 + \nu_2)/2$ ) and the detuning parameters  $\Delta_- = \omega_1 - \omega_2$ ,  $\Delta_+ = \omega_1 + \omega_2 - 2\omega_L$  [3].

The eigenstate coefficients of Hamiltonian (1) are depicted in Fig. 1 in terms of the different control parameters of the model. We have used some of the experimental data reported in [1] and some other input values that reveal interesting scenarios. The eigenenergy spectra (not shown) indicate that indeed the energy difference between the entangled states shown in Fig. 1(a), for  $\Delta_- = 2320$  MHz (vertical line), is about 3 GHz, in agreement with the spectral results of [1]. However, notice that as the laser coupling is increased, there is a more significant contribution from all the basis states to the system eigenstates, thus producing (e.g., for  $\Delta_- = 2320$  MHz) the superpositions  $\alpha_{00}|00\rangle + \alpha_{01}|01\rangle + \alpha_{10}|10\rangle + \alpha_{11}|11\rangle$  with weight coefficients  $\alpha_{ij}$  as illustrated in Fig. 1(a). This means that for strong laser pumping,  $\alpha_{00}$  and  $\alpha_{11} \neq 0$  in contrast to the entangled sub- and super-radiant states reported in [1]. As shown in Fig. 1, such entangled states  $|\Psi_a\rangle$  and  $|\Psi_s\rangle$  [4] can indeed be created but for a different parameter window (e.g., for  $\Delta_-/V_{12} > 500$ ). Figure 1 also shows that, for a fixed  $V_{12}$ , the bigger the energy difference  $\omega_1 - \omega_2$ , the easier one can achieve a ‘disentangling effect’, where the system’s eigenstates can become, to a very good approximation, equal to the computational basis states. This is illustrated as a function of the detuning parameter in Figs. 1(c) and (d).

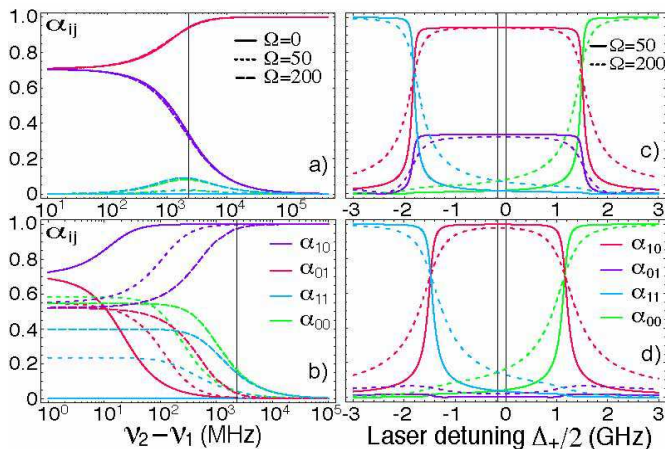


FIG. 1: Eigenstate coefficients  $\alpha_{ij}$  of the coupled system in the absence and presence of laser pumping as a function of  $\Delta_-$ , and detuning  $\Delta_+/2$ . The weights of the basis states of the 4-level system have been plotted for  $V_{12} = 950$  MHz (graphs (a) and (c)) and for  $V_{12} = 10$  MHz ((b) and (d)).  $\Delta_- = 2320$  MHz in graphs (c) and (d). Notice the difference in eigenstates behaviour for  $\Delta_- \sim V_{12}$ , and  $\Delta_-/V_{12} \gg 1$  [4].

As a result of the dipole-dipole interaction between molecules, the system exhibits resonant cooperative absorption of light [5], thus allowing simultaneous excitation by absorption of two-photons; we represent the spontaneous decay of such excitations by the rate  $\Gamma_{12} = \Gamma_{21}$ .

It is not difficult to calculate the general expressions for the  $d$ - $d$  interaction strength and the incoherent decay rate  $\Gamma_{12}$  [6]. In the near field ( $r_{12} \ll \lambda_L$ ) the interaction energy and the incoherent decay rate are given by  $V_{12} = \frac{3\sqrt{\Gamma_1\Gamma_2}}{8\pi\epsilon_0^3}[\hat{\mathbf{d}}_1 \cdot \hat{\mathbf{d}}_2 - 3(\hat{\mathbf{d}}_1 \cdot \hat{\mathbf{r}}_{12})(\hat{\mathbf{d}}_2 \cdot \hat{\mathbf{r}}_{12})]$ , and  $\Gamma_{12} = \sqrt{\Gamma_1\Gamma_2} \hat{\mathbf{d}}_1 \cdot \hat{\mathbf{d}}_2$ , and hence the maximum (minimum) strengths are obtained for parallel (perpendicular) dipole moments.  $z = nk_0 r_{12}$ ,  $\Gamma_i = \frac{nA_{12;i}}{2} = n\omega_i^3 \|\mathbf{d}\|^2 / (3\epsilon_0 hc^3)$ , where  $A_{12;i}$  ( $i = 1, 2$ ) are the Einstein coefficients in vacuum, and  $\hat{\mathbf{d}}_i$  and  $\hat{\mathbf{r}}_{12}$  are unit vectors along  $\mathbf{d}_i$  and along  $\mathbf{r}_{12}$ . The presence of the dielectric modifies the molecules radiative decay rates which in turn implies a shift in the molecular energy levels. The vacuum frequencies are now modified and hence the phase velocity of light waves in the dielectric medium is given by  $c/n(\omega) = \omega/k(\omega)$ .

We describe the full molecular quantum dynamics by solving the master equation for the Lindblad operator [7], thus taking into account all the possible excitation decay channels  $\Gamma_i$ , and  $\Gamma_{ij}$ . In particular, Ref. [1] reports an energy shift in the fluorescence spectrum associated with the upper level  $E_\epsilon$  of  $\Delta_+/2 \simeq -160$  MHz (see the central resonance of Fig. 2(a)), where the steady-state density matrix element  $\rho_{ee,ee} \equiv \langle e_1 e_2 | \rho | e_1 e_2 \rangle$  displays the observed shift ( $\Delta_+/2 = -160$  MHz, vertical dashed line). This effective shift can be attributed to the Lamb shifts of the three states  $|\Psi_a\rangle$ ,  $|\Psi_s\rangle$  and  $|\Psi_\epsilon\rangle$ . Decay channel interference modifies the decay rates of the first two states [1] (and hence their Lamb shifts) away from the uncoupled values. As a consequence, the doubly-excited state is effectively displaced from where it would be expected, given the energies of the lower two levels. The Lamb shifts can be calculated by taking into account self-interactions and by renormalizing to remove quadratic divergences [5, 8] from  $\Lambda_i = -\frac{\|\mathbf{d}_i\|^2 \omega_i^3}{3\pi\epsilon_0 hc^3} \int n(\omega) [(\omega + \omega_i)^{-1} + (\omega - \omega_i)^{-1}] d\omega$ . A detailed calculation for the experimental set-up reported in [1] shows that  $\Delta_\epsilon = \Lambda_\epsilon - \Lambda_s - \Lambda_a \simeq -178$  MHz, a result that is in good agreement with the observed value, as is shown by the inset of Fig. 2 where the fluorescence around this excitation energy is plotted for both the theoretical (solid line) and the measured (dashed line) values as a function of the laser detuning  $\Delta_+/2$ . As we show below, the  $\Delta_\epsilon$  shift is clearly useful for QIP; even more so because it can be tailored by means of an appropriate engineering of the structural and optical properties of the molecular set-up. Different strengths  $\Delta_\epsilon$  are shown in Fig. 2(b) where the expected fluorescence spectra is plotted as a function of the laser detuning  $\Delta_+/2$ . The result that additional energy shifts appear in the spectra is viewed here as a meaningful resource for performing molecular two-qubit logic gates and therefore for quantum computing purposes. Although we have focused on the experimental data reported in [1], other parameter windows and different molecular systems can certainly be explored in the light of our results.

The splittings in the energy spectrum of the interacting system can be used to induce a conditional dynamics between the two subsystems (e.g., a laser with  $\lambda_L \simeq 578$  nm and linewidth  $\Delta\nu \simeq 1$  MHz can be suitable [1]). Figure 1 displays the eigenstate coefficients in the absence and presence of laser pumping for different interaction strengths  $V_{12}$ . For  $\ell_i = 0$ , the energy separation between  $|\Psi_s\rangle$  and  $|\Psi_a\rangle$  is  $\sqrt{\Delta_-^2 + 4V_{12}^2}$  [4] and hence molecules of equal transition energies ( $\Delta_- = 0$ ) have  $c_1 = c_2 = 1$  and the corresponding symmetric and antisymmetric states become the maximally entangled states (MES)  $\frac{1}{\sqrt{2}}(|e_1g_2\rangle \pm |g_1e_2\rangle)$ , as can also be seen in Figs. 1(a) and (b). Otherwise ( $\omega_1 \neq \omega_2$ ), the degree of molecular entanglement can be manipulated by controlling the ratio  $V_{12}/\Delta_-$ . This can be experimentally done by means of applying a differential Stark shift via an external inhomogeneous electric field to select different values of the detuning  $\Delta_-$  or by directly tuning the dipole-dipole interaction by means of changing the separation  $r_{12}$  and/or by using a medium with different dispersive properties. This means that a rich spectra of entangled symmetric and antisymmetric states can be generated by modifying the eigenstate coefficients. It follows from [4] that  $\alpha_1 = \sqrt{(Y+1)/2Y}$ ,  $\alpha_2 = \sqrt{(Y-1)/2Y}$  ( $Y \equiv X/\Delta_-$ ), then, if the system's ratio  $V_{12}/\Delta_- \ll 1$ ,  $\alpha_2 \approx V_{12}/\Delta_-$  ( $c_i/\sqrt{2} \equiv \alpha_i$ ): the bigger the difference in the transition energies (compared to  $V_{12}$ ) the more disentangled the intermediate states become.

The effective shift  $\Delta_\epsilon$  described above implies that the resonant frequency for transitions between the basis states  $|g_i\rangle$  and  $|e_i\rangle$  of one qubit *depends* on the state of the neighbouring qubit: the energy difference between states  $|\Psi_a\rangle$  and that of  $|\Psi_g\rangle$  is different from the one between states  $|\Psi_\epsilon\rangle$  and  $|\Psi_s\rangle$  due to  $\Delta_\epsilon$  and  $V_{12}$  [4]. Thus, in the scenario  $V_{12}/\Delta_- \ll 1$ , we can naturally construct the two-qubit CNOT gate  $U_{\text{CNOT}}: |m\rangle \otimes |n\rangle \mapsto |m\rangle \otimes |m \oplus n\rangle$ . Hence, the logic operation  $|e_1\rangle |g_2\rangle \mapsto |e_1\rangle |e_2\rangle$  can be achieved by illuminating the input qubit system with a  $\pi$ -pulse of energy  $\Omega_{12} = \omega_2 - \delta + \Delta_\epsilon$  (say, a  $\pi_{\Omega_{12}}$ -pulse), where  $\delta = V_{12}^2/\Delta_-$ . This is illustrated, for experimentally attainable values [1], in Fig. 3(a) where the system's initial state  $|e_1g_2\rangle$  is induced to evolve onto the final state  $|e_1e_2\rangle$  via the application of a  $\pi_{\Omega_{12}}$ -pulse, thus realizing a quantum CNOT gate in 1.25 ns. In the absence of dissipative channels the gate operation exhibits a perfect fidelity (see below), whereas the inclusion of realistic decay rates shows the appearance of small weight contributions arising from the populations  $\rho_{gg,gg}$  and  $\rho_{ge,ge}$  (curves at the bottom of Fig. 3(a)). This, however, can be further controlled by means of choosing different  $\Delta_\epsilon$ ,  $V_{12}/\Delta_-$ , and laser strengths to improve the gate fidelity. Conversely, if the role of the control qubit is to be performed by the second qubit, the gate operation  $|g_1\rangle |e_2\rangle \mapsto |e_1\rangle |e_2\rangle$  can be realized via a  $\pi_{\Omega_{21}}$ -pulse of frequency  $\Omega_{21} = \omega_1 + \delta + \Delta_\epsilon$ . The energy selectivity of such a CNOT gate is thus deter-

mined by  $\Delta_-$ ,  $\Delta_\epsilon$  and  $V_{12}$ , and typical operation time scales can be gathered from Figs. 2 and 3 for different parameter windows. The complimentary unitaries in SU(2) required to build a universal set of gates can be achieved by inducing appropriate Rabi oscillations of the corresponding dipole operator expectation value  $\langle \hat{\mathbf{d}} \rangle = \langle \hat{P}_{12}\mathbf{d}_{12} + \hat{P}_{21}\mathbf{d}_{21} \rangle$ . Thus, single qubit control can be performed by tailoring the energy and length of applied laser pulses to induce distinct Rabi oscillations.

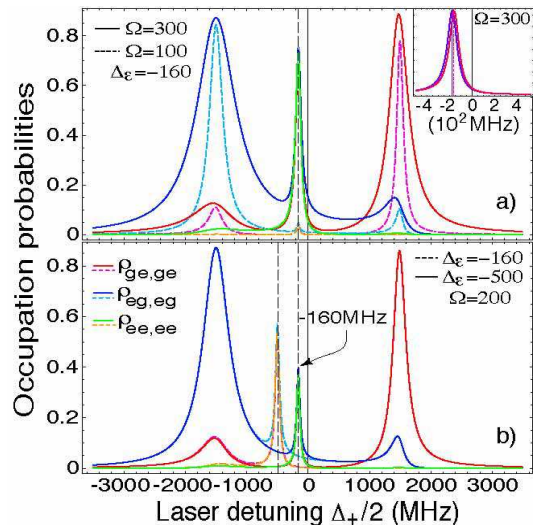


FIG. 2: Steady-state density matrix elements as a function of the laser detuning parameter  $\Delta_+/2$ . The occupation probabilities give the structure of the resonance fluorescence spectrum, as is shown in a) for different excitation intensities  $\ell_i$ , and in b) for different effective shifts  $\Delta_\epsilon$ ;  $\ell_i \equiv \Omega$ ,  $\Gamma_i = 50$  MHz,  $\Gamma_{12} = 9$  MHz,  $\Delta_-/2 = 1160$  MHz, and  $V_{12} = 950$  MHz.

The scenario considered previously exploits the diagonal shifts  $\Delta_\epsilon$  by means of focusing on a particular parameter window. However, even for arbitrary  $V_{12}/\Delta_-$  ratios one can still perform entangling gates that enable universal QC. By writing the interaction Hamiltonian of Eq. (1) as  $\hat{H}_{12} = \hbar V_{12}[\hat{\sigma}_x \otimes \hat{\sigma}_x + \hat{\sigma}_y \otimes \hat{\sigma}_y] \equiv \hat{H}_{xy}$ , one can define an *optimal* entangling gate  $U_{xy}$  for the  $d$ - $d$  interaction by simply letting the system evolve under  $\hat{H}_{xy}$  for a time  $t_{xy} = \pi/4V_{12}$ . By means of the self-adjoint operator  $\hat{H}_{\vec{\mu}} = \sum_i \mu_i \hat{\sigma}_i \otimes \hat{\sigma}_i$ ,  $\hat{U}_{\vec{\mu}} \equiv \exp(-i\hat{H}_{\vec{\mu}})$  provides, up to LU, a decomposition for *any* two-qubit gate and thus the  $d$ - $d$  interaction has associated  $U_{xy}$ :  $|m\rangle \otimes |n\rangle \mapsto i^{|m-n|} |n\rangle \otimes |m\rangle$  as its ‘natural’ entangling gate [9]. This gate, equivalent to a combination of CNOT and SWAP, plus LU, are a universal gate-set. This means that, provided one has access to performing sufficiently fast LU operations, one could always exploit the  $d$ - $d$  interaction for universal QC. Typical switching times for the experimental data analyzed here can be in the sub-picosecond time scale ( $\sim 1/1000$  the fastest decay rate).

We calculate the steady-state density matrix elements

in the computational basis as a function of the laser detuning  $\Delta_+/2$ . Fig. 2(a) shows a strong enhancement of the two-photon resonance (TPR) as the strength of the laser coupling is increased (for  $V_{12} = 950$  MHz). As the  $d$ - $d$  coupling determines the size of the TPR, the weaker the interaction the more difficult the detection of the TPR fluorescence peak. Fig. 2(b) shows effectively that an increase in  $\Delta_\epsilon$  has associated with it a further TPR shift that could then be observed in the fluorescence spectrum, as predicted above. The asymmetric shape of the resonance lines arises from the destructive and constructive interference between the system's excitation decay channels  $|\Psi_g\rangle \mapsto |\Psi_a\rangle \mapsto |\Psi_\epsilon\rangle$ , and  $|\Psi_g\rangle \mapsto |\Psi_s\rangle \mapsto |\Psi_\epsilon\rangle$ , which in turn is also reflected in the observed linewidth difference between the left and right peaks (Fig. 2), a hallmark of Dicke's subradiance and superradiance.

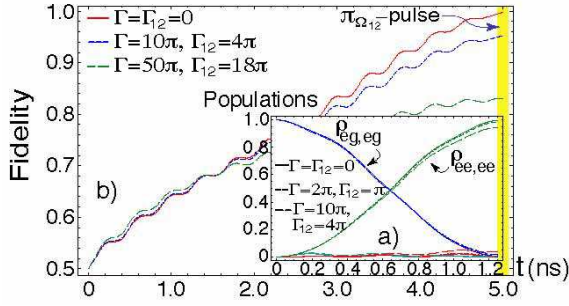


FIG. 3: (a) CNOT gate operation: a  $\pi_{\Omega_{12}}$ -pulse is applied in order to generate the conditional logic  $|e_1g_2\rangle \mapsto |e_1e_2\rangle$ . The corresponding populations are shown as a function of time in the absence and presence of dissipative channels.  $\Delta_+/2 = -1319$  MHz,  $\Delta_- = -2320$  MHz,  $\ell_i \equiv \Omega = 200$  MHz,  $\Delta_\epsilon = 160$  MHz, and  $V_{12} = 50$  MHz. (b) Fidelity (see text) in the generation of the MES  $\frac{1}{\sqrt{2}}(|g_1g_2\rangle + |e_1e_2\rangle)$ . The bar signals the end of the applied  $\pi_{\Omega_{12}}$ -pulse and indicates a measure of the actual entangled state achieved in the absence and presence of dissipation. Input parameters are as before except for  $\Omega = 50$  MHz. Decay rates are given in  $10^6 \text{ s}^{-1}$  units.

The quality of the gates discussed here depends on the ability to control the relevant structural and external parameters. An indication of gate performance is the quality of the maximally entangled states they produce. Due to decoherence, any attempt to generate a MES  $|\psi_m\rangle$  in practice creates a mixed state  $\rho$ . In Fig. 3(b) we plot the corresponding fidelity  $\mathcal{F} \equiv \sqrt{\langle \psi_m | \rho | \psi_m \rangle}$  for  $|\psi_m\rangle \equiv \frac{1}{\sqrt{2}}(|g_1g_2\rangle + |e_1e_2\rangle)$ . The initial state is taken to be  $\frac{1}{\sqrt{2}}(|g_1\rangle + |e_1\rangle)|g_2\rangle$  (this can be achieved by starting in the system's ground state and then applying a  $\pi/2$  pulse at energy  $\omega_1$ ), and hence  $|\psi_m\rangle$  can be generated by applying a  $\pi_{\Omega_{12}}$ -pulse. Figure 3(b) gives the fidelity between  $|\psi_m\rangle$  and  $\rho$  in the presence of dissipative interactions. Clearly, zero decay gives a perfect fidelity ( $\mathcal{F} = 1$ ), but the action of dissipative processes (as described in [7]) gives  $\mathcal{F} \lesssim 1$ , as shown in Fig. 3(b) by the bar signaling

the end of the applied  $\pi_{\Omega_{12}}$ -pulse. We have considered the rather non-optimistic ratio  $\frac{V_{12}}{\Delta_-} \sim 2 \times 10^{-2}$  but smaller ratios could indeed be experimentally achievable and hence improved fidelities can be obtained in conjunction with tailored  $\Delta_\epsilon$ , and laser field values. Our numerical experiments consider a setup and energy scales that have been measured in the laboratory [1] thus providing a significant step towards proof-of-principle experiments that can be undertaken with currently available technology.

Although of a different physical origin, we stress that the main ideas discussed here can also be applied in the context of the technologically important self-assembled coupled quantum dot molecules [10, 11] and biomolecular systems [12]. Summarizing, we have given a detailed prescription for molecular conditional quantum dynamics that can be implemented with modest experimental requirements by tailoring control parameters such as excitation frequencies, spontaneous decay rates, interaction strengths, and external laser pumping. Furthermore, we have explained the quantum mechanical origin of the TPR energy-level shift and we have highlighted its relevance to QIP protocols. We have shown that the performance of a molecular quantum gate can be adjusted by varying the value of this shift.

We thank V. Sandoghdar for valuable correspondence. JHR is supported by EPSRC as part of the Foresight LINK Award *Nanoelectronics at the Quantum Edge*.

\* On leave from Centro Internacional de Física, A. A. 4948, Bogotá, Colombia (j.reina-estupinan@physics.ox.ac.uk).

- [1] C. Hettich *et al.*, Science **298**, 385 (2002).
- [2] D. Petrosyan and G. Kuriziki, Phys. Rev. Lett. **89**, 207902 (2002), also quant-ph/0411188.
- [3] The effective Hamiltonian reads (in the product basis):

$$\hat{H} = \hbar \begin{pmatrix} -\frac{\Delta_+}{2} & \ell_2 & \ell_1 & 0 \\ \ell_2 & -\frac{\Delta_+}{2} & V_{12} & \ell_1 \\ \ell_1 & V_{12} & \frac{\Delta_+}{2} & \ell_2 \\ 0 & \ell_1 & \ell_2 & \frac{\Delta_+}{2} + \Delta_\epsilon \end{pmatrix}. \quad (2)$$

- [4] These eigenfunctions read (for  $\ell_i = 0$ ):  $|\Psi_g\rangle = |00\rangle$ ,  $E_g = -\frac{\Delta_+}{2}$ ;  $|\Psi_a\rangle = \frac{1}{\sqrt{2}}(-c_1|01\rangle + c_2|10\rangle)$ ,  $|\Psi_s\rangle = \frac{1}{\sqrt{2}}(c_1|10\rangle + c_2|01\rangle)$ ,  $E_a = -E_s = -\frac{X}{2}$ ;  $|\Psi_\epsilon\rangle = |11\rangle$ ,  $E_\epsilon = \frac{\Delta_+}{2} + \Delta_\epsilon$ , where  $c_1 = \sqrt{4V_{12}^2/X(X + \Delta_-)}$  and  $c_2 = \sqrt{4V_{12}^2/X(X - \Delta_-)}$ ;  $X \equiv \sqrt{\Delta_-^2 + 4V_{12}^2}$ .
- [5] G. S. Agarwal, Springer Tracts in Modern Physics Vol. 70, edited by G. Höhler (Springer-Verlag, Berlin, 1974).
- [6] In frequency (Hz) units:  $\Gamma_{12} = \mathcal{C}_{12}\{[\hat{\mathbf{d}}_1 \cdot \hat{\mathbf{d}}_2 - (\hat{\mathbf{d}}_1 \cdot \hat{\mathbf{r}}_{12})(\hat{\mathbf{d}}_2 \cdot \hat{\mathbf{r}}_{12})] \frac{\sin z}{z} + [\hat{\mathbf{d}}_1 \cdot \hat{\mathbf{d}}_2 - 3(\hat{\mathbf{d}}_1 \cdot \hat{\mathbf{r}}_{12})(\hat{\mathbf{d}}_2 \cdot \hat{\mathbf{r}}_{12})] \frac{\cos z}{z} - \frac{\sin z}{z^3}\}$ ; and  $V_{12} = \mathcal{C}_{12}\{-[\hat{\mathbf{d}}_1 \cdot \hat{\mathbf{d}}_2 - (\hat{\mathbf{d}}_1 \cdot \hat{\mathbf{r}}_{12})(\hat{\mathbf{d}}_2 \cdot \hat{\mathbf{r}}_{12})] \frac{\cos z}{z} + [\hat{\mathbf{d}}_1 \cdot \hat{\mathbf{d}}_2 - 3(\hat{\mathbf{d}}_1 \cdot \hat{\mathbf{r}}_{12})(\hat{\mathbf{d}}_2 \cdot \hat{\mathbf{r}}_{12})] \frac{\sin z}{z^3} + \frac{\cos z}{z^2}\}$ , where  $\mathcal{C}_{12} \equiv \frac{3\sqrt{\Gamma_1\Gamma_2}}{8\pi}$ .
- [7]  $\dot{\rho} = -\frac{i}{\hbar}[H, \rho] + \sum_{ij} \frac{\Gamma_{ij}}{2}(2S_i^- \rho S_j^+ - \rho S_i^+ S_j^- - S_i^+ S_j^- \rho)$ , with  $i, j = 1, 2$ ,  $\Gamma_{ii} = \Gamma_i$ , and  $\Gamma_{ji} = \Gamma_{ij}$ .

- [8] P. W. Milonni *et al.*, Phys. Rev. A **59**, 4259 (1999); J. Mod. Opt. **42**,1991 (1995).
- [9] K. Hammerer *et al.*, Phys. Rev. A **66**, 062321 (2002).
- [10] J. H. Reina *et al.*, Phys. Rev. A **62**, 012305 (2000);
- B. W. Lovett *et al.*, Phys. Rev. B. **68**, 205319 (2003).
- [11] S. A. Crooker *et al.*, Phys. Rev. Lett. **89**, 186802 (2002).
- [12] J. L. Herek *et al.*, Nature **417**, 533 (2002).